# INSPECTION INTERVALS FOR FRACTURE-CRITICAL STEEL BRIDGES BASED ON FATIGUE AND FRACTURE LIFE-CYCLE COST ASSESSMENT

HUSSAM MAHMOUD

## BIOGRAPHY

**Dr. Hussam Mahmoud** is an Associate Professor of civil engineering at Colorado State University (CSU). He is also the Director of the Structural Laboratory at CSU. Dr. Mahmoud's research experience is in the area of fatigue and fracture assessment of steel structures, life cycle analysis of engineered systems, and resilient infrastructure.

**Mr. Akshat Chulahwat** is a graduate research assistant at Colorado State University. His research experience is in the area of life-cycle and resilience.

**Mr. Mazin Irfaee** is a graduate research assistant at Colorado State University. His research experience is in the area of fatigue and fracture.

## SUMMARY

Fatigue cracks in steel bridges are considered a nuisance as they require periodic inspection and repair. Although the cracks are typically characterized by stable propagation rate, the scatter in fatigue performance is difficult to quantify and could be on the order of thousands or even millions of cycles. If left unattended, the cracks could grow to reach critical length and threaten the integrity of the structure. The concern over structural safety is further intensified for fracture critical bridges, resulting in a federal mandate of bi-annual hands-on inspection and causing financial strains on funding available to transportation departments. Given the scatter in fatigue data and the substantial cost associated with inspection and repair, the use of probabilistic life-cycle cost analysis could, therefore, provide a viable alternative for the development of maintenance and management programs for steel bridges. In this paper, a framework for probabilistic life-cycle assessment is created and applied for minimizing the life-cycle cost of a steel twin tub bridge. First, a detailed finite element model of the bridge is developed and probabilistic relationships of crack growth versus number of cycles are generated. Second, a life-cycle framework is devised and used to optimize the cost and schedule associated with repair and inspection of the bridge over its service life without comprising on safety. The results demonstrate that viability of using this framework for ensuring the lowest possible cost for addressing fatigue issues in steel bridges over a service life chosen by the bridge owner while ensuring safe operation of the bridge.

# INSPECTION INTERVALS FOR FRACTURE-CRITICAL STEEL BRIDGES BASED ON FATIGUE AND FRACTURE LIFE-CYCLE COST ASSESSMENT

Hussam Mahmoud, Akshat Chulahwat, and Mazin Irfaee

## 1. Introduction and Background

In the first half of the 20th century few bridge failures caused nationwide concern over vulnerability of steel bridges. As a consequence, the American Association of State Highway and Transportation Officials, AASHTO, started to classify bridges more strictly so that those vulnerable to complete collapse can be identified. A new category for fracture critical bridges (FCB) was introduced. A FCB is defined as a bridge with at least one fracture critical member (FCM). Whereas a FCM is defined as a "component in tension whose failure is expected to result in the collapse of the bridge or the inability of the bridge to perform its function" (1). This implied that, two-girder steel bridges would be classified as nonredundant and fracture critical (FC). As a result, bi-annual hands-on inspection were mandated. In the United States, 11% of the bridges are classified as fracture critical, 83% of which comprise of two girder steel bridges (2). The cost implications of the bi-annual inspection mandate are enormous and imposes financial strain on taxpayer's money and federal funding. This problem is further aggravated by the fact that most bridges in the United States were built around the 1960s and many of them have shown significant signs of aging and deterioration over the years. Demolition and replacement of these bridges is an expensive alternative. Therefore, relying on cost-effective maintenance and repair strategies in prolonging the life of a bridge, is ever pressing. The development of these cost-effective strategies requires the formulation of life-cycle models, which need to include both epistemic and aleatory uncertainties associated with the specific bridge in question. Several researchers have developed comprehensive probabilistic life-cycle frameworks for optimal maintenance budget allocation regarding deteriorating structures (3,4,5,6,7). These studies have quite effectively highlighted the importance and need for efficient life-cycle strategies to establish well-balanced intervention schedules that consider various economic and safety requirements while taking into account uncertainties associated with the time-dependent structural performance. Accurate assessment of structural performance is key for reliable life-cycle evaluation. With recent advancement in computing technologies, researchers and engineers can now develop detailed finite element models (FEM) that represent the true behavior of the structure in question. Life-cycle optimization frameworks combined with detailed FEM models can not only further improve the accuracy of maintenance strategies, but also give better understanding of the inherent redundancies within a system.

In this paper a steel-twin box-girder bridge is considered for optimal maintenance assessment by combining a detailed FEM model with a life-cycle cost optimization strategy. Two models for the bridge are developed – with and without lateral bracings. The FEMs are first used to conduct probabilistic fatigue crack growth analysis, which include assessment under mixed modes fatigue loading. The crack propagation rate corresponding to the most conservative case is used as an input for the life-cycle framework. Within the life-cycle framework, costs associated with only repair and inspection are included. The optimization is used in conjunction with Monte Carlo simulation to optimize on maintenance schedule while accounting for the uncertainties associated with the FEMs.

## 2. Finite Element Model

The steel box-girder bridge, considered in this study, is located on W 44$^{th}$ Avenue crossing I-25 highway in Denver, CO. A suitable 3D finite element model of the bridge is constructed, which is further used to conduct probabilistic risk assessment and life-cycle cost analysis, as discussed in the subsequent sections.

### *3.1 Geometry*

Two models are built of the aforementioned bridge – (a) with bracings, and (b) without bracings between the girders. The bridge model is constructed to be 105.77 meters (347 ft) in length and 14.33 meters (47 ft) in width. Other geometric details of the bridge are shown in Fig. 1. The finite element software ABAQUS ver. 6.14 is used for model formulation and analysis.

The model comprises of 34 single parts, which are assembled into 76 instances. A mix of three key element types – (a) line (Beam) element (b) shell element, and (c) solid element are used to simplify the model and reduce processing time. Line elements are used for the bracings, solid element for partition of the girder at the crack location, and shell elements for the remaining parts of the model. In addition, all steel connections are defined in the model as welded connections and interaction between concrete slab and girders is defined as fully composite.

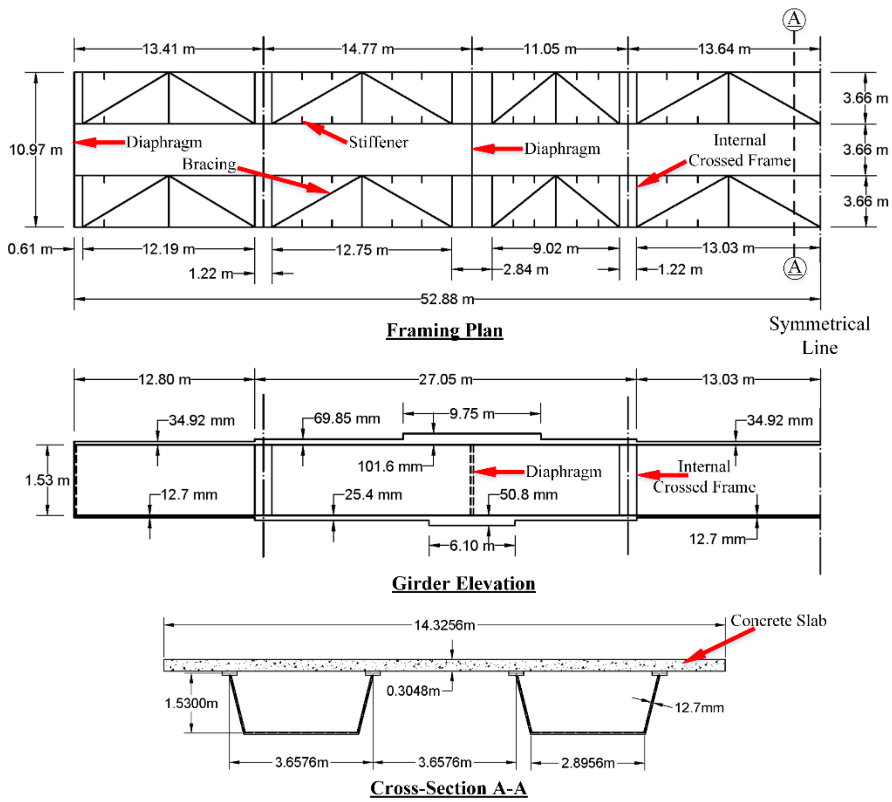


Fig. 1. Bridge geometric details

### *3.2 Material Properties*

The model is constructed of primarily two materials – (a) steel of grade 50 (A572) with yield stress of 345 MPa, ultimate stress of 448 MPa, elasticity module of 200,000 MPa and a Poisson ratio of 0.3 (b) reinforced concrete with compressive strength of 40 MPa, an elasticity module of 25,131 MPa, and Poisson ratio of 0.26. The material properties of the reinforced concrete are calculated using rule of mixtures. This is essentially a weighted mean used to predict the properties of a composite material made up of continuous and unidirectional fibers. Eq. (1) defines the principle of rule of mixtures.

$$X_{eq} = \frac{1}{V_{total}} \sum_{1}^{n} V_n * X_n \qquad (1)$$

Where $X_{eq}$ is the equivalent property, $n$ is the number of material combine, $V_n$ is the volume of material n, $X_n$ is the property for material $n$, and $V_{total}$ is the total volume for all materials used. Since the analysis is extended to plastic range the reinforced concrete slab is modeled to include reinforced steel rebars. Concrete damage plasticity (CDP) model from Jankowiak & Lodygowski (8) is used to evaluate the equivalent plastic strain as limit state for the collapse.

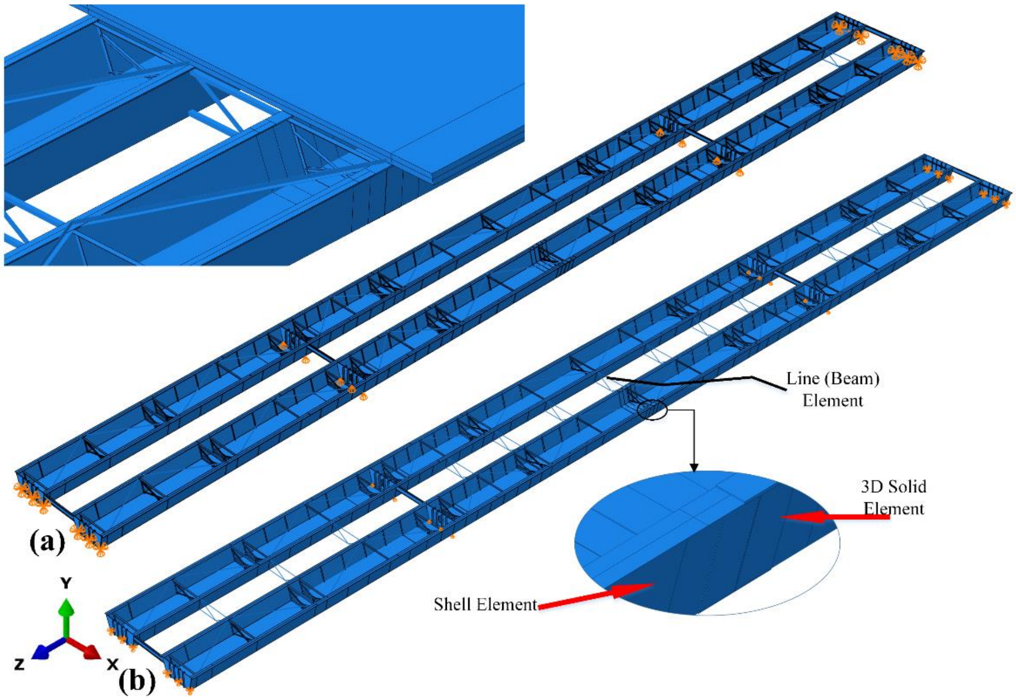


Fig. 2. Bridge mesh details

### *3.3 Mesh Formulation*

Three types of mesh element are used in the model – 3-node quadratic beam line element (B22), 8-node curved thick shell element with reduced integration (S8R) and 20-node quadratic brick element with reduced integration (C3D20R). The line elements are used for the bracings and diaphragms, the shell elements for the tubs and the concrete slab, and the brick elements for the mesh surrounding the crack region in the tub girder. This allowed for proper capturing of stresses in the tub through the thickness for accurate predictions of crack growth. In addition, a recursive mesh analysis is conducted to assess the optimum mesh size around the crack region, which converged to be 20 mm.

### *3.3 Crack Propagation*

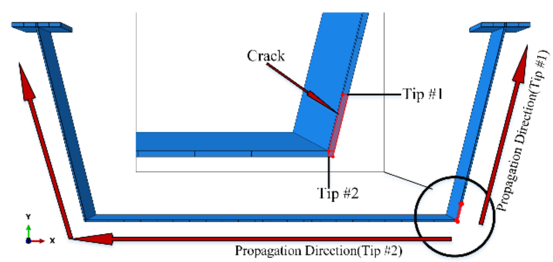


Fig. 3. Initial crack location and propagation direction

The critical crack location is identified at a welded stiffener connection (Category C) located at midspan on one of the bridge girders, where the web and bottom flange are connected (Fig. 3), due to the maximum positive bending moment observed. An initial crack length of 127 mm (5 inches) is assumed, with increments of 127 mm. The initial crack location and the directions of each tip of crack is shown in Fig. 3. Due to asymmetrical positioning of the two crack tips, the crack propagation rate is different for both tips as the crack propagates in the bottom flange plate and vertically in the web. The Paris Law is used to approximate the difference in propagation rates between the two crack tips, since the number of cycles at each crack increment would be the same.

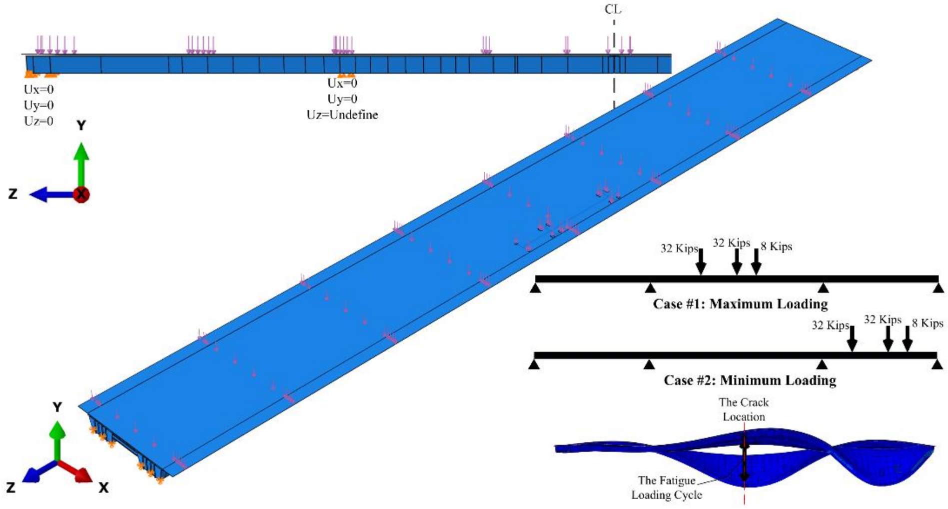


Fig. 4. Loading configurations and boundary conditions

## *3.4 Load Configuration*

The loading configuration is assigned to the model based on the AASHTO, 2012 requirements for fatigue and fracture analysis. Specifically, an HL-93 is considered with dynamic load allowance of 15% since the analysis is conducted statically. Furthermore, the loading on the bridge is divided to define the fatigue life and the fracture for different crack length. Two loading configurations are defined to represent the fatigue loading cycle, as shown in Fig. 4 (i.e. case #1 and case #2). The location of loads is determined based on the truck locations specified in accordance with AASHTO, 2012 to produce maximum positive and negative bending moments. The results from this loading case are utilized in the life-cycle analysis. To evaluate the potential for collapse in the presence of full fracture of one of the girders, another loading configuration is defined, which comprised of similar configuration as the first case (maximum bending) along with additional load due to self-weight and lane load. The specified lane load is 0.8677 KN/m (0.64 kips/ft) for 3.0 m (10 ft) width lane. The loads are magnified with additional factor of safety of 1.5 for dead load, 1.75 for live load, and 1.15 for dynamic allowance.

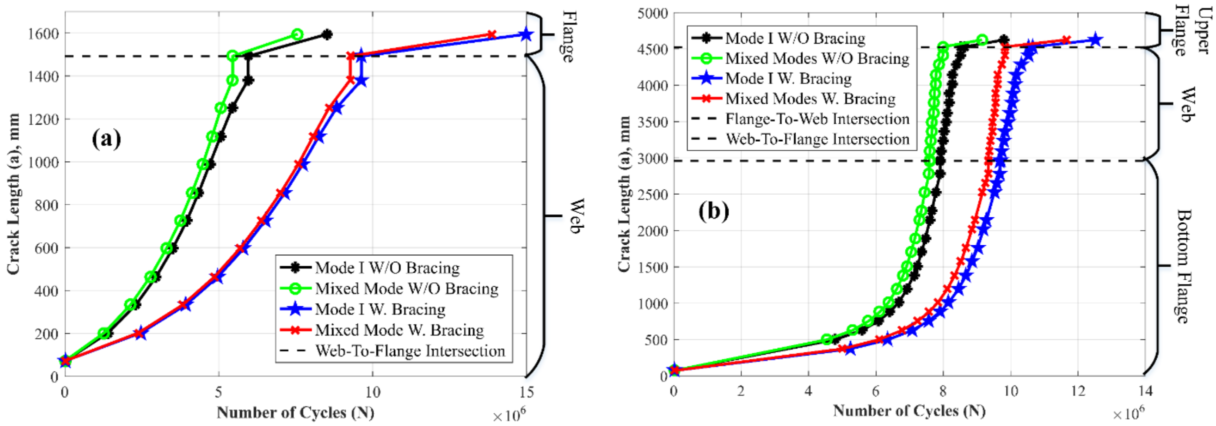


Fig. 5. Number of Cycles Vs. Crack Length (Propagation Rate) for different modes of loading considered (a) Tip #1 and (b) Tip #2

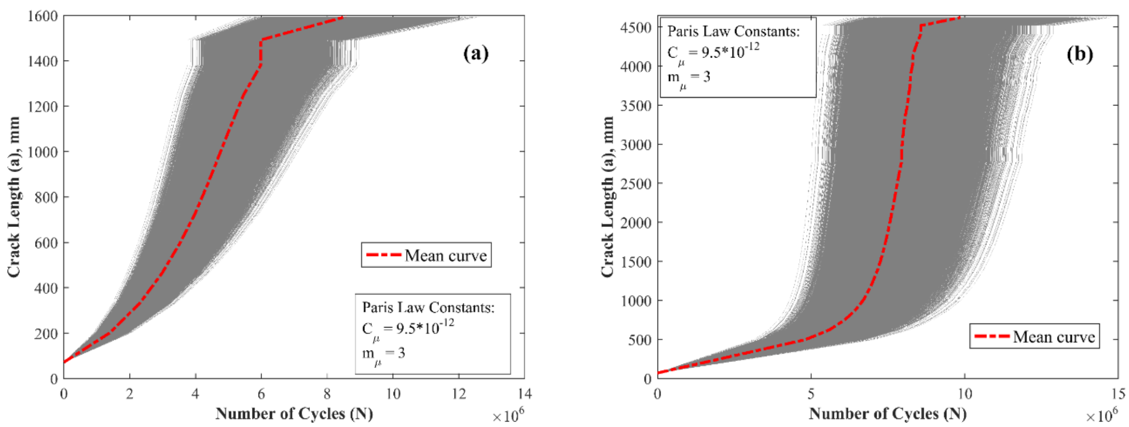


Fig. 6. Propagation Rate with Variation in Paris Law Constants (a) Tip #1 and (b) Tip #2

# 3. Fatigue and Fracture Assessment

Stress intensity factor (SIF) corresponding to different crack lengths are evaluated and used in the Paris Law for the evaluation of crack growth rate. Paris hypothesized that the range in stress intensity factor, ΔK, governs fatigue crack growth. Experimental da/dN versus ΔK data typically exhibits a sigmoid here is a ΔK threshold, $\Delta K_{th}$, below which cracks will not propagate. The Paris law is fit to the linear part (on a log–log scale) above $\Delta K_{th}$. At relatively high ΔK levels, the crack growth rate accelerates, as the fatigue crack growth is accompanied by some ductile tearing or increments of brittle fracture in each cycle.

$$\frac{da}{dN} = C(\Delta K)^m \tag{2}$$

where $C$ and $m$ are material constants.

Utilizing the Paris Law, the analysis is performed twice to evaluate the effect of considering only mode I loading versus mixed modes on the resulting fatigue crack growth. A similar pattern of SIFs is observed for first and mixed mode analysis results for lower crack lengths, since the second and third modes showed relatively low SIF values. At higher crack lengths, some variation is observed, however, resulting in a difference of approximately 7-10% in fatigue life (cycles to failure). Due to the limited scope of this study, the fracture results for each mode are not explicitly discussed. The Paris Law is used to evaluate the relation between crack propagation and total number of cycles to failure (Fig. 5). As expected, the model with braces shows higher fatigue life (approximately 20%-30%) than the model without bracings.

To account for uncertainties associated with fatigue crack growth, variation in the Paris Law constants, $C$ and $m$, are assumed in accordance with previous studies and guidelines (9,10). Normal distributions with a mean of $C_\mu$ = 9.5x10$^{-12}$, $m_\mu$ = 3 and standard deviation $C_\sigma$ = 0.25x10$^{-12}$, $m_\sigma$ = 0.03 are utilized. Using Monte-Carlo simulation for $N$ = 100,000 iterations the distribution in fatigue life as a function of crack length is calculated (Fig. 6). A clear variation in fatigue life is observed, especially for crack tip #2.

# 4. Life-Cycle Cost Optimization

Inspection and maintenance are required at regular intervals to prolong the service life of a structure. However, the intervals at which these inspections and maintenance should be specified require careful deliberation as minimizing life-cycle cost of structures while ensuring structural safety through proper resource allocation is a key consideration (11). In this section an optimization framework is proposed and discussed. The framework utilizes life-cycle cost information, along with the probabilistic curves obtained in the previous section, to calculate optimal inspection/repair routine.

## *5.1 Parameters*

Assessment of life-cycle cost requires a sufficient understanding of the events involved in maintaining and prolonging the life of the structure. This may include but not limited to inspection, repair and maintenance. Depending on the nature of the method adopted for each activity, the life-cycle cost would vary significantly. In this study, only inspection and repair are considered. The total cost of an inspection-repair event is estimated by Eq. (3),

$$C_t(t) = R[C_i(t,k) + P_d(k, d(t)).C_r(t)] \qquad (3)$$

where $C_i$ is the total inspection cost of type $k$ inspection at time $t$, $C_r$ is the total repair cost, $P_d$ is the probability of detection of the type of inspection method used and $R$ is the cost inflation factor to a particular year. Depending on the crack size and inspection type, sometimes critical cracks would not be detected during the inspection phase; thus $P_d$ is introduced to account for this uncertainty.

The cost inflation factor is defined by Eq. (4), where $r$ is the annual inflation rate and $t$ is the time. There exist several types of inspection methods, each with its own distinct accuracy.

$$R = \frac{1}{(1+r)^t} \qquad (4)$$

The total inspection and repair cost are defined as shown in Eq. (5) and (6) as the sum of their direct ($C_i^d$ and $C_r^d$) and indirect ($C_i^{in}$ and $C_r^{in}$) costs.

$$C_i(t,k) = C_i^d(t,k) + C_i^{in}(t,k) \qquad (5)$$

$$C_r(t,k) = C_r^d(t) + C_r^{in}(t) \qquad (6)$$

Both the direct and indirect inspection costs are dependent on the type of method used. Eq. (7) describes the indirect inspection cost as a function of time taken by the specific method ($t_i$) and the closure cost per day ($C_c$), which is independent of the method type.

$$C_i^{in}(t,k) = t_i(t,k).C_c \qquad (7)$$

In case of repair costs, both direct and indirect components are related to the crack length $d$, which in turn vary with time probabilistically and is defined by cumulative sum of crack length of tip#1 ($d_1$) and tip#2 ($d_2$) as per Eq. (8). The direct repair cost is defined as the product of crack length and repair cost per unit length ($C_w$) as shown in Eq. (9). The indirect cost is defined as the product of closure cost per day, crack length and amount of time taken to repair crack of length $d$ as per eq. (10).

$$d(t) = d_1(t) + d_2(t) \qquad (8)$$

$$C_r^d(t) = C_w.d(t) \qquad (9)$$

$$C_r^{in}(t) = t_r.d(t).C_c \quad (10)$$

*5.2 Optimization*

The optimization framework implemented in this study entails the use of a non-linear heuristic optimization - 'CMA-ES' (Covariance Matrix Adaptation Evolution Strategy) (12) to calculate the optimal inspection and repair schedule. The optimization generates a sample population of solutions, tests the efficacy of each sample, creates an improved sample from previous one and continues the process until either convergence is achieved or until a desired number of runs are completed. As observed from the discussion in the previous section, one of the key parameters required for optimization is the functional relation between time and crack length ($d(t)$). By assuming an average number of load cycles per day ($N_{avg}$) the curves in Fig. 6 are used to obtain the necessary curves from Eq. (10), where $N_{max}$ is the maximum cycles observed.

$$t_{sl} = \frac{N_{max}}{365.N_{avg}} \quad (10)$$

Because of uncertainties in variation of crack length with time (or number of cycles), Monte Carlo is combined into the fitness equation of the optimization, as given by Eq. (11), where $t_{sl}$ is the target service life, $n_t$ is the number of iterations for Monte Carlo, $d_{th}$ is the threshold crack length not to be exceeded, $\beta$ is a penalty factor and $sgn(x)$ is the signum function which determines the sign of $x$. The optimization problem can be described as shown below:

**Optimization Variable:** $k = \{\lambda_1, \lambda_2 \dots \lambda_{t_{sl}}\}$, such that $\lambda_i \in \{0,1\}$. A value of 1 representing an inspection repair and 0 representing otherwise. For this study, only one type of inspection is considered but the framework can incorporate several types at the same time as desired.

**Constraints:** $t_{i+1} - t_i \geq 2$, such that $\lambda_i = 1$. The interval between any consecutive inspection-repair events needs to be at least 2yrs. Secondly, the threshold crack length ($d_{th}$) should not be exceeded during the service life.

**Objective function:** Minimize $F$

$$F = \frac{1}{n_t}\sum_{n=1}^{n_t}\left[\sum_{t=1}^{t_{sl}} C_t(t) + \beta[1 - sgn(d_{th} - d(t))]\right] \quad (11)$$

An important thing to note is that the crack length curves obtained from the FEM model are valid only to a certain number of cycles. It is assumed that as each time a repair is performed, the crack length is reset back to its initial value. In reality, this should result in shorter life for the new repair in comparison to the original detail. However, this was not accounted for in this study. Thus, based on the inspection-repair schedule pattern, a modified $d(t)$ curve is derived for each case.

*5.1 Results*

Life-cycle cost optimization is conducted using the framework discussed on the bridge model with bracings. The optimization is performed to obtain optimal inspection-repair schedule for each case, such that the service life can be extended to a desired target life, which is considered to be 70 yrs in this study. The mixed mode case is considered as the test case since it showed the lowest fatigue life among all modes. The crack length curves ($d(t)$) are derived based on separate propagation rates of tip#1 and tip#2 (Fig. 6). The threshold crack length is decided upon based on the correlation between crack length and maximum displacement of girder. Based on the increase in displacement with respect to crack length two values are selected for threshold crack length ($d_{th}$) – (1) 1000 mm and (2) 2000 mm. The average load cycle is assumed to be 1000 cycles/day and 2000 cycles/day. In this study, only visual inspection is considered and the probability of detection is assumed to be 1, due to large size of the crack. The corresponding values of other input parameters are listed in Table 1.

**Table 1.** Optimization input parameters

| Definition | Variable | Value | Unit |
|---|---|---|---|
| Inspection direct | $C_i^d$ | 20,000 | $ |

| | | | |
|---|---|---|---|
| cost | | | |
| Inspection time | $t_i$ | 3 | days |
| Closure cost | $C_c$ | 3000 | $ |
| Inflation rate | $r$ | 3 | % |
| Repair cost | $C_w$ | 10 | $/mm |
| Repair time | $t_r$ | 0.002 | mm/days |
| Penalty factor | $\beta$ | $10^{10}$ | - |
| Monte Carlo iterations | $n_t$ | 1000 | - |

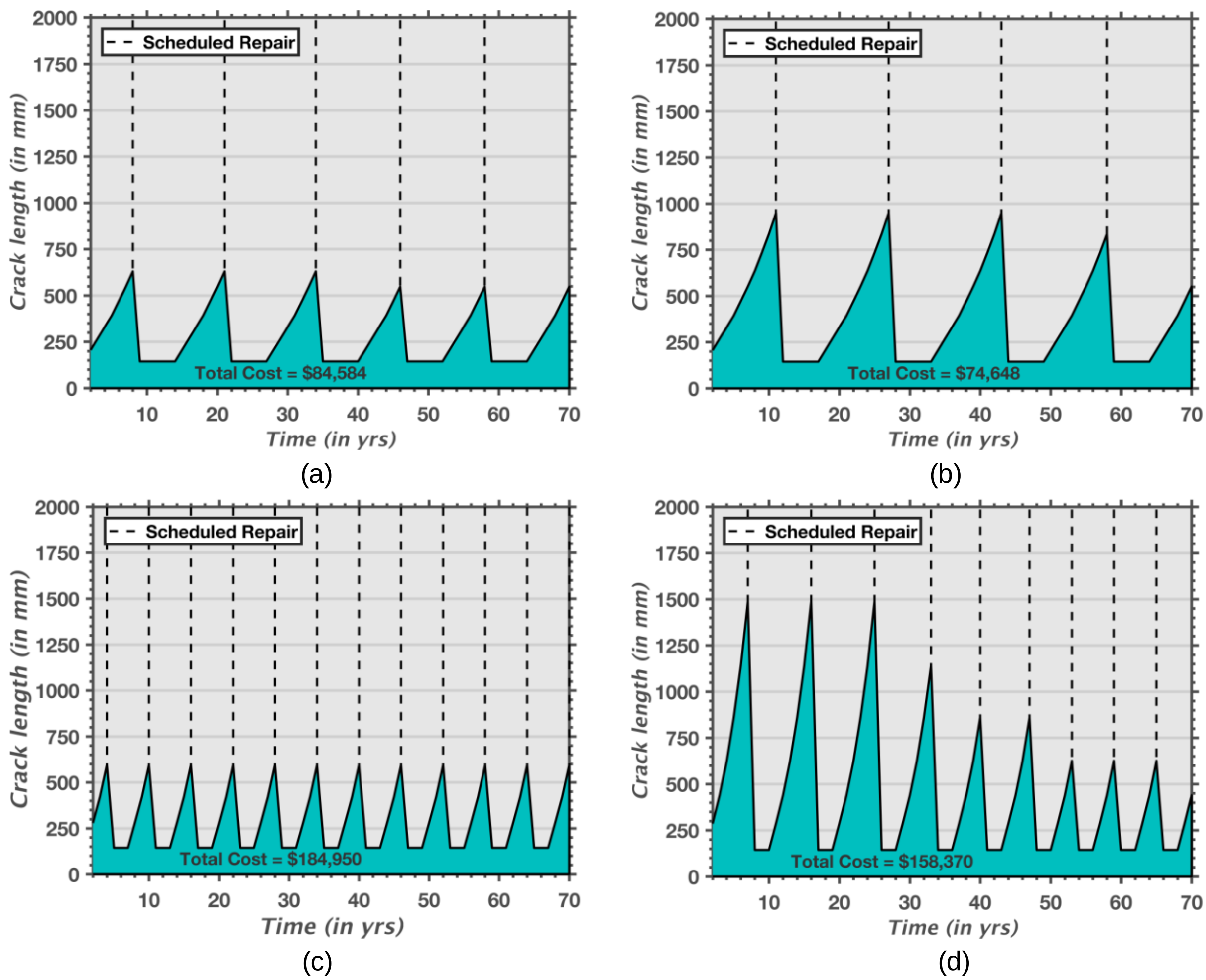


Fig. 7. Life-cycle cost optimization results for different values of ($d_{th}$, $N_{avg}$) (a) (1000 mm, 1000 cycles/day) (b) (2000 mm, 1000 cycles/day) (c) (2000 mm, 2000 cycles/day) (d) (2000 mm, 2000 cycles/day)

The results for the four test cases are shown in Fig. 7. The figure clearly shows the variation in the scheduled inspection and repair schedule not to be confined to the bi-annual mandate. The figure presents the variation in net crack growth (crack tip#1 + tip#2) with time under a given maintenance schedule. After each inspection-repair event the crack length is reset, and certain time is required for crack initiation and growth again. This period of inactivity is represented in the figures as the constant crack length versus time after each repair. The time to initiation for the Category C detail is calculated for the 2 cases of average cycles ($N_{avg}$) assumed, and their respective values are found to be 2.71yrs (for $N_{avg}$ = 2000 cycles/day) and 5.54yrs (for $N_{avg}$ = 1000 cycles/day). The lifecycle cost is observed to be maximum when the frequency of loading cycle is high, and the allowed crack threshold length is low (Fig. 7(c)). Higher frequency of loading results in faster crack propagation rate, as observed from the increase in slope for cases (c) and (d). In case (a) and (b) low loading cycles result in higher initiation time and low rate of crack growth, as a result, the optimization larger intervals for maintenance to keep the lifecycle cost low. The threshold crack length selected also governs the interval between maintenance events. However, its effect is not as pronounced as compared to the loading cycles. The effect of threshold crack length is observed to be much higher between cases (c) and (d) than (a) and (b), suggesting that its effect would play a much important role at higher loading cycles. For the optimal schedule patterns observed in all test cases, the frequency of maintenance increased with time, which was probably due to the cost inflation.

In this study, only a single crack location is considered of interest; however, in case of multiple crack locations by controlling multiple threshold values favorable failure sequences can be promoted. This would allow engineers to exploit any inherent redundancies present in the system. This further highlights the motivation behind this study. Given the substantial number of bridges of United States in their later stages, the need for efficient maintenance strategies are critical for ensuring minimal cost without compromising on safety.

## 5. Discussion

In this study, life-cycle cost analysis of a steel twin box-girder bridge was performed using probabilistic fracture mechanics. A computationally efficient, yet comprehensive, FEM model was developed to evaluate fatigue crack propagation life and failure mode. Critical crack location was identified from the model and its corresponding stress intensity factor are evaluated to define a relationship between crack length and fatigue life using Paris Law. The uncertainties associated with material properties are also accounted within the analysis. *The functional relation of fatigue life with crack length was further used in conjunction with a life-cycle cost framework to conduct optimization and identify optimal schedule patterns so as to minimize the total cost over the lifetime of the structure*. The following summarizes key discussion points of this study:

- The FEM model with bracings showed higher fatigue life than the model without bracings, as the bracings provided redundancy and redistributed the loads.
- Higher modes i.e. second and third mode showed relatively lower SIF values than first mode. As a result, mixed mode and first mode showed similar behavior for low crack lengths, but a slight deviation for higher crack lengths.
- Uncertainty in material properties had an effect on crack propagation rate, which in turn resulted in large scatter in total lifecycle cost.
- The load cycles had a significant effect on the total life-cycle cost, as expected. Crack length threshold had an inversely proportional effect, however, the effect was relatively mild.
- The optimal schedules obtained for different cases showed similar pattern. The inspection-repair interval was observed to be higher in the early years, followed by reduction in the interval for later years.
- Optimization was observed to be sensitive to crack propagation rate. Since in this study only one critical crack location was considered, the accuracy of the discussed framework can be significantly improved by considering multiple cracks.
- Costs associated only with inspection and repair were considered in the life-cycle cost framework. The framework can be improved by including costs pertaining to maintenance delay and monitoring.

# References


1. AASHTO. (2012). AASHTO LRFD Bridge Desigin Specification. Washington, DC. http://doi.org/978-1-56051-523-4
2. Connor, R., Dexter, R., & Mahmoud, H. (2005). NCHRP Synthesis 354: Inspection and Management of Bridges with Fracture-Critical Details. *Transportation Research Board.*
3. Estes, A. C. & Frangopol, D. M. (1999). Repair optimization of highway bridges using system reliability approach, *Journal of Structural Engineering*, 125(7), 766-775.
4. Faber, M. H. & Sorensen, J. D. (2002). Indicators for inspection and maintenance planning of concrete structures. *Journal of Structural Safety*, 24, 377-396.
5. Kong, J. S. & Frangopol, D. M. (2003). Life-cycle reliability-based maintenance cost optimization of deteriorating structures with emphasis on bridges, Journal of Structural Engineering, 129(6), 818-828.
6. Mahmoud, H. and Chulahwat, A., and Riveros, G. (2017) “Fatigue and Fracture Lifecycle Cost Assessment of a Miter Gate with Multiple Cracks”, *Engineering Failure Analysis*, doi.org/10.1016/j.engfailanal.2017.09.008.
7. Stewart, M. G., Estes, A. C. & Frangopol, D. M. (2004). Bridge deck replacement for minimum expected cost under multiple reliability constraints. *Journal of Structural Engineering*, 130(9), 1414-1419.
8. Jankowiak, T., & Lodygowski, T. (2005). Identification of parameters of concrete damage plasticity constitutive model. *Foundations of civil and environmental engineering*, *6*(1), 53-69.
9. Mahmoud, H., & Riveros, G. (2013). Fatigue reliability of a single stiffened ship hull panel. *Engineering Structures*, *66*, 89-99.
10. BS-7910. (1997). Guide to methods for assessing the acceptability of flaws in metallic structures. *BSI Standards Publication*.
11. Estes, A. C., Frangopol, D. M. & Foltz, S. (2004). Updating reliability of steel miter gates on locks and dams using visual inspection results. *Engineering Structures*, 26 (3), 319-333.
12. Hansen, N. (2011). The CMA Evolution Strategy: A Tutorial.